Aerodynamics of High Speed Trains Passing by Each Other

Kozo FUJII* and Takanobu OGAWA**

*The Institute of Space and Astronautical Science, Yoshinodai 3-1-1, Sagamihara, Kanagawa, 229 Japan

**Shimizu Corporation, Etchujima 3-4-17, Koto-ku, Tokyo, 135 Japan

ABSTRACT

A three-dimensional flow field induced by two trains passing by each other inside a tunnel is studied based on the numerical simulation of the three-dimensional compressible Euler/Navier-Stokes equations formulated in the finite difference approximation. Domain decomposition method with the FSA(fortified solution algorithm) interface scheme is used to treat this moving-body problem. The computed resluts show basic characteristic of the flow field created when two trains passing by each other. History of the pressure distributions and the aerodynamic forces acting on the trains are mailnly discussed. The results indicate that the phenomenon is complicated due to the interaction of the flow induced by two trains. Strong side force occurs between the two trains when the front portion of the opposite train passes by. It fluctuates rapidly and maximum suction force occurs when two trains are aligned side by side. The results also indicate the effectiveness of the present numerical method for moving boundary problems.

1. INTRODUCTION

Transportation vehicles are becoming faster and faster and the speed of recent trains is now more than 250 km/h, that corresponds to the Mach number more than 0.2. At this high speed, compressibility of air may not be negligible. A lot of aerodynamic problems can be imagined at such high speeds. For instance, aerodynamic noise, aerodynamic load when trains run in the tunnel and trains pass by each other are the typical ones. Complicated aerodynamic loads may act on train bodies and it is not easy to predict them because relative position of the train bodies changes in time and therefore the flow field becomes very unsteady. Future trains under planning will increase their speeds substantially, and if so, aerodynamic forces become still larger and may cause structural fatigue and affect the passengers comfort. Only a few studies have been conducted on these flow problems in the past. They are mostly the analysis based on the empirical theory or field measurement[1,2]. The details of the flow properties and the variation of the unsteady aerodynamic forces are not well understood. The difficulty mainly comes from the fact that trains are moving in time relative to the ground. It is almost impossible to physically realize some of the important flow fields accurately in the wind tunnel experiment. Experiments without considering relative movement of the train are possible, but the flow properties obtained by the experiments are limited and not accurate. In addition, the maximum velocity of the trains is at most Mach number 0.2 or so due to the limitation of the experimental

apparatus. More detailed information of the flow field is necessary for the design of future trains that may run at higher speeds.

Recent progress of the computer capability and numerical methods allows us to simulate such flow fields even in three dimensions and computational research works on train aerodynamics have been reported[3-5] as high-speed trains become one of the important engineering topics in many countries. The present authors have been investigating two-dimensional[6] and three-dimensional[7] problems for the train entry to the tunnel using a domain-decomposition method. The result showed the capability of the computational approach on the moving body problems such as train entry to the tunnel . In the present paper, the three-dimensional flow field where two trains pass by each other inside a tunnel is simulated in three dimensions. Domain decomposition method with the interface scheme called Fortified Solution Algorithm (FSA)[8] is used to handle this moving zonal problem. Computational region, and therefore, the computer load is halved by a new boundary condition adopted under the assumption that two trains run at the same speed. The time sequence of the flow field and the history of the aerodynamic forces acting on the trains are investigated. The result shows the detailed aerodynamics that occur when two trains pass by each other at high speed in a tunnel.

2. NUMERICAL METHOD

2.1 Basic Equations

The basic equations are the unsteady three-dimensional compressible Euler equations.

$$\partial_t \hat{Q} + \partial_\xi \hat{E} + \partial_\eta \hat{F} + \partial_\zeta \hat{G} = 0 \quad (1)$$

$$\hat{Q} = \begin{bmatrix} \rho \\ \rho u \\ \rho v \\ \rho w \\ e \end{bmatrix}, \hat{E} = \begin{bmatrix} \rho U \\ \rho uU + \xi_x p \\ \rho vU + \xi_y p \\ \rho wU + \xi_z p \\ (e+p)U - \xi_t p \end{bmatrix},$$

$$\hat{F} = \begin{bmatrix} \rho V \\ \rho uV + \eta_x p \\ \rho vV + \eta_y p \\ \rho wV + \eta_z p \\ (e+p)V - \eta_t p \end{bmatrix}, \hat{G} = \begin{bmatrix} \rho W \\ \rho uU + \zeta_x p \\ \rho vU + \zeta_y p \\ \rho wU + \zeta_z p \\ (e+p)U - \zeta_t p \end{bmatrix}$$

The pressure is expressed by the equation of state for an ideal gas as,

$$p = (\gamma-1)\left(e - \frac{1}{2}(u^2 + v^2 + w^2)\right) \quad (2)$$

Pressure wave created by the trains can be captured by the Euler equation and viscous effect on the tunnel wall is not important for this problem. However, separation of the flow near the train body surface may change the effective body configuration and may influence on the unsteady pressure field. Therefore, the thin-layer Navier-Stokes equations are locally used in the zone for the train body.

The basic equations are written in the generalized coordinate system with the time metrics terms included. Thus, the motion of the grid is expressed in the term ξ_t, η_t, ζ_t which are constant in the present paper.

2.2 Fortified Solution Algorithm (FSA)

The FSA took the basic concept from the idea of Fortified Navier-Stokes(FNS) approach that was originally developed by Van Dalsem and Steger[9] to improve the performance of Navier-Stokes algorithms by using fast auxiliary algorithms that solve subsets of the Navier-Stokes equations. One of the present authors used this FNS concept as an interface scheme and developed a zonal method for a steady-state vortical flow problem[10]. Since the basic equations can not necessarily be the Navier-Stokes equations, this zonal method is now called FSA (Fortified Solution Algorithm) zonal method[11]. In the FSA approach, solution to the subset equations are used as added forcing terms to the basic algorithm in the appropriate flow regions. When the FSA is applied to the Euler equations, the basic equations are rewritten as

$$\partial_\tau \hat{Q} + \partial_\xi \hat{E} + \partial_\eta \hat{F} + \partial_\zeta \hat{G} = \chi (\hat{Q}_f - \hat{Q}) \qquad (3)$$

The right-hand side term is the fortifying(forcing) term. The solution is fortified to be $\hat{Q}_f$ when the switching parameter χ is set to be sufficiently large. For the region that χ values are set zero, the equations go back to the original Euler equations. By adding the forcing terms and modifying the solution procedure, we can overlay the known solution $\hat{Q}_f$ onto the solution $\hat{Q}$ in the appropriate region. Usually the solution obtained with finer grids or other zones having higher priority is implemented on $\hat{Q}_f$. When having higher priority, the solution of the other zones at the previous time step is taken as $\hat{Q}_f$ in this computation.

Modification of the existing solution algorithm is simply to change I matrix to I $(1 + h\chi)$ matrix with the consideration that χ can become large without concern for large factorization errors. In the case of the LU-ADI factorization time integration algorithm that is used in the present simulation, the modification can be written as follows. In the original LU-ADI algorithm,

the ADI operator for each direction, for instance the operator for the ξ-direction can be written as,

$$I+h\delta_\xi\hat{A} = T_\xi(I - h\hat{D}^-_{Aj} + h\delta^b_\xi\hat{D}^+_A)(I + h|\hat{D}_A|)^{-1} \times (I + h\hat{D}^+_{Aj} + h\delta^f_\xi\hat{D}^-_A)T_\xi^{-1} \quad (4)$$

This operator is modified to add the forcing term as follows.

$$T_\xi(I\,(1+h\chi) - h\hat{D}^-_{Aj} + h\delta^b_\xi\hat{D}^+_A)(I\,(1+h\chi) + h|\hat{D}_A|)^{-1} \times (I\,(1+h\chi) + h\hat{D}^+_{Aj} + h\delta^f_\xi\hat{D}^-_A)T_\xi^{-1} \quad (5)$$

When χ is zero, Equation (5) becomes Eq.(4). By putting the inversion of $I\,(1 + h\chi)$ between each ADI operator to avoid the large factorization errors, $\hat{Q}^{n+1} = Q_t$ is realized when χ is large. The modification of the right-hand side is to add source terms. The required implementation for this algorithm is just to add the source term to the right hand side and to set the distribution of χ parameter, whatever kind of domain decomposition (such as patched grid or overset) grid may be used.

2.3 Spatial Discretization

The basic equations are discretized in the finite difference fashion. In the right-hand side, convective terms are evaluated using flux difference splitting by Roe. The MUSCL interpolation is used for the higher-order extension. Metrics terms include the time derivatives to take care of the grid movement. All the details about the evaluation of the right-hand side except the treatment of Fortified source terms shown above can be found in the paper by Fujii and Obayashi[8].

3. COMPUTATIONS AND DISCUSSIONS

3.1 Flow Configuration

Figure 1 shows the schematic picture of the flow field. Two trains having the same shape move at the same speed of Mach number 0.22 (270km/h) in the opposite direction. The railroad is double tracked and the train runs on the left track. The length scale is nondimensionalized by the tunnel hight. The width of the train is 0.34 and the space between the two trains is 0.11. The trains are located 4.0 apart from each other at the beginning. The coordinate is defined as the point of train crossing to be x=0.0. Figure 2 shows the cut of the flow field in the horizontal plane. In this plane, the flow field is point symmetric about the center point under the condition that the same trains cross each other at the same speed. In other words,

$$\begin{bmatrix} \rho \\ \rho u \\ \rho v \\ \rho w \\ e \end{bmatrix}_{r'} = \begin{bmatrix} \rho \\ -\rho u \\ -\rho v \\ \rho w \\ e \end{bmatrix}_{r} \qquad (6)$$

is valid, where r' is the point of symmetry of r as illustrated in Fig. 2. Only the velocities, u and v are anti-symmetric. Using this assumption, only the upper left half of the flow field is solved, that reduces both the grid points and the computer time.

In the present computation, viscous effect is only taken into account in the flow field around the train. Thin-layer Navier-Stokes equations are used in the train zone and the bottom zone. The Reynolds number based on the tunnle hight is set to be 1.0×10^{7}. LU-ADI time

integral algorithm is employed, since the time stepping in the explicit algorithms are too restricted by the CFL condition in a viscous computation. It has been shown that the speed of wave propagation can be captured correctly by implicit methods if Courant number defined in the inviscid region is taken to be small. The time step is taken sufficiently small (0.002 non-dimensional time) to resolve the unsteadiness of the flow field. The computation required about 50 hours on VP200 supercomputer at the ISAS.

It would take much computational time if the trains were located far away from each other at the beginning. Instead, the quasi steady-state solution that is obtained for the trains located in a finite distance from each other is used as an initial condition. Figure 3 shows the flow region for the steady state computation. Only the negative x region is computed. At the inflow boundary (right boundary of the hatched region), point symmetry condition is imposed. Thus, the effect of the opposite train is approximately taken into account in the initial flow field near the train, which avoids non-physical pressure wave created when the solution process starts.

3.2 Computational Grids

The flow field is divided into 4 zones, the tunnel zone, the zone around the train (TRAIN ZONE), the bottom of the train (BOTTOM ZONE) and the interface zone. Since the train and bottom zones move at the train speed, the position of the grids in the moving zones relative to the tunnel gird should be computed at each time step and zone-to-zone interpolation is necessary at the zonal boundaries. The interface zone that is composed of simple square grids was prepared to save the computer time necessary for finding the position of the moving grid relative to the tunnel grid. This interface zone also moves with the train. The coefficients necessary for the interpolation between the moving grids and this interface square grid do not change in time because all these grids move at the same speed. Since the interface grid is a Cartesian-like square grid, interpolation between this interface grid and tuunel grid becomes simple, and thus the computer time is very much saved. The total grid points are approximately

265,000 points. The details of the TRAIN ZONE and the BOTTOM ZONE are shown in Fig. 4. The grid points of the TRAIN ZONE are distributed by the hyperbolic grid generation method and the other grid points are generated algebraically.

3.3 Computed Results

To help understanding the result, relative position of the trains at several time stations is presented in Fig. 5. At t=-9.09, the trains start moving with the steady-state solution as an initial condition. At t=0.0, both the train noses come to the point x = 0.0. At t=5.68, both trains are aligned side by side. At t=11.36, both the train rear noses are located at x = 0.0 and crossing is finished. Top view of the pressure contour plots on the ground as well as the train surface is shown in Figs. 6(a)-(g). When the trains are approaching, the pressure between the trains increases(t=-1.09). However, as soon as the trains begin to cross each other (t=0.91), the pressure at the front nose(stagnation) of the trains begins to decrease. At the same time, the pressure at the outer side of the train front nose becomes low. The velocity vector plots (not shown here) indicate strong flow from the inside high pressure region to the outside low pressure region exists over the train. When the bodies of the trains are crossing each other(t=1.91), the pressure near the shoulders between the train bodies strongly decreases. The pressure at the nose front still decreases. When the trains are crossing, the flow is accelerated since the cross sectional area inside the tunnel becomes small. The low pressure region becomes larger as the trains cross each other further. Particularly, the pressure at the shoulders of the trains becomes low. When the trains are located almost side by side (at t=5.91), the pressure at the shoulders strongly decreases again. Then, the trains go away from each other (t=7.91) and the pressure at the front nose recovers as it was before the crossing.

The time history of the pressure on the side surface facing to the opposite train is plotted in Fig. 7 to show the fluctuation of the pressure on the train surface. The point of measurement is longitudinal center of the body as is also shown in the figure. The broken lines drawn in the

figure indicate the time when the front and rear noses pass the point, respectively. The pressure starts increasing just before the front nose of the opposite train passes the point and has high peak at the time of its passing. Immediately after the pressure peak, the pressure suddenly decreases and becomes lowest when the shoulder of the opposite train passes the point. It is interesting to know that the pressure decrease is much larger and more rapid than the pressure increase. Therefore, strong suction force works on the inside of the trains and pulling side force occurs as will be seen below. When the rear nose of the train passes the point, reversal phenomenon occurs and the pressure decreases first, then increases. The fluctuation due to the rear nose is much smaller than that of the front nose due to the fact that the wake of the train changes the effective body geometry. Although the experimental data for the comparison is not available, the qualitative nature of the computed result agrees well with the field observation of the rapid train (260km/h and 210km/h) currently under operation in Japan[2].

The aerodynamic forces acting on the train are important for passengers comfort and safe train operation. The history of the aerodynamic forces while the train crossing is described below. All the coefficients are normalized by the projected cross sectional area of the train. See Fig. 4 again for the relative train position. Figure 8(a) shows the history of the drag coefficient, C_D. When the trains start crossing, the drag force decreases since the pressure at the front nose decreases as described above. It decreases until the shoulder crosses the shoulder of the opposite train. Then the drag force recovers a little as the stagnation pressure recovers, but again starts decreasing as the front nose approaches the rear shoulder of the opposite train. Two local minima of the drag force are observed at t=2.0 and 5.0, when the front nose of the train passes by the shoulder of the opposite train.

The history of the lift coefficient, C_L is plotted in Fig. 8(b). The C_L increases when the crossing begins at t=0.0, keeps almost constant value until t=5.0, and then decreases. The pressure on the upper surface of the train becomes low during the crossing. The pressure on the

bottom surface also decreases (although not shown here), but not as strong as the upper surface. Therefore the lift force acts on the train while crossing. However, the fluctuation of C_L is much smaller compared to the other forces.

The side force, C_Y, is plotted in Fig. 8(c). The positive C_Y indicates the force to pull the trains apart. As the trains come close, C_Y becomes large due to the high pressure between the front noses. Then, it decreases until the shoulder of the train meets the shoulder of the opposite train. The C_Y, then increases and has a peak at about t=3.0. To find out the mechanism of this C_Y behavior at around t=3.0, side force distribution at t=2.1 and 3.1 are plotted in Figs. 9(a) and (b). Note that the size of the arrows corresponds to the local side force working toward inside rather than outside. Main reason may be the pressure recovery at the front nose that pushes the train apart(See also the drag peak at t=3.0). At the same time, negative side force acting on the outside of the train becomes smaller as the pressure level between the train and the tunnle wall recovers. This also contributes to make a small peak in the side force distribution at t=3.0. After that, C_Y decreases again. This is again due to the fact that the pressure surrounded by the two trains becomes low. When the trains are located side by side (t=5.68), the pressure between the trains strongly decreased and the high pressure regions around the train noses do not contribute to C_Y any more, and thus C_Y becomes the minimum value and the side forces to put the trains closer work on the trains. After that, as the trains move away from each other, C_Y becomes small.

The history of the three moments are plotted in Figs. 8(d)-(f). The yawing moment shown in Fig. 8(d) is mainly discussed. The definition of the moment is illustrated in Fig. 8. When the trains are approaching each other, the high pressure works on the inside face of the front noses and it increases the positive C_{M_Y}. At t=1.0 or so when both shoulders meet, it has the maximum value and starts decreasing because low pressure region at the shoulders becomes large. At about t=3.0, the C_{M_Y} becomes minimum. At this moment, low pressure region exists between

the forward part of the trains as can be seen in Fig. 6(d), and it induces large negative yawing moment. Although the low pressure region between the two trains still increases, the yawing moment defined at the center of the body becomes small because suction force acts on both directions. Another small positive peaks appear at t=5.0 and 8.0 and negative peak appears at t=6.5. The first peak may occur due to the fact that the contribution of the high pressure region near the front nose creating negative moment diminishes as the front nose in the opposite train passes away the straight portion of the train. The last two peaks may be due to the size and level of the low pressure region between the two trains. However, such C_{M_Y} fluctuations are much smaller compared to the first positive and negative peaks. Figure 8(e) shows the pitching moment. Note that the moment is defined as the center of the body to be an origin also in the vertical direction. The pitching moment has the similar trend as the drag force. The rolling moment is plotted in Fig. 8(f). The rolling moment is important for the passengers' comfort and the train stability. It shows almost the same trend as the side force plotted in Fig. 8(c). The mechanism for the side force described above with the help of the mechanism of the lift history explains the trend of the rolling moment.

All the plots do not have dimensional values. To get the feeling of the practical values, the dimensional physical values are computed by assuming the train size and speed. The side force, for instance becomes a few hundreds kg per square m's and thus becomes order of ton's in total even for this small train. On the other hand, the lift force is at most hundreds of kg's which may not be noticeable. Of course, the train shape used here is an ideal one and more realistic simulations taking the additional body elements into account will be necessary to accurately evaluate the aerodynamic forces acting on the train.

In summary, the mechanism of the aerodynamic forces is governed by the high stagnation pressure at the nose and strong low pressure region near the shoulder of the train. The location of the nose and the shoulder relative to those of the opposite train basically explains the trend of

aerodynamic forces and moments. That means the improved design of the frontal part of the train may reduce the strong side force and yawing moments that occur during the crossing of two trains. The frontal part of the train is conventionally designed considering the reduction of the aerodynamic drag without considering any interaction with the opposite train. However, the result here indicates that it should be designed with the interaction of the opposite train taken into account. A good design in the sense of small drag does not necessarily means a good design for all.

The present paper discusses the aerodynamic characteristics of two trains passing by in a tunnel. The effect of the tunnel has not been discussed at all. It is imagined that flow phenomenon is almost the same except that the pressure between the train and the tunnel wall becomes low during the process and it may affect the interaction.

4. CONCLUSIONS

The flow field induced by two trains passing by each other has been numerically simulated using the Euler/Navier-Stokes equations. Domain decomposition method was used to handle this moving boundary problem. The computed result showed that complicated flow pattern appears. Strong side force acts on the train and it has several positive and negative peaks. The other forces and moments also show the large fluctuations. It was revealed that the aerodynamic forces and moments strongly depends on the relative position of the trains. Especially, the location of the nose and the shoulder plays an important role. The result also indicates that the nose area of the train should not be designed solely on the drag reduction basis. The design of the nose region may influence the strength of the aerodynamic loads on the train while passing by each other. Another conclusion is that computational methods to these moving-body unsteady-flow problems may give us a lot of informations that would never be obtained in the experiments

and are useful for understanding the flow field.

REFERENCES

1. S. Ozawa, Aerodynamic Loads on Trains," Text prepared for JSME lecture series. No.900-37, June. (1990) (in Japanese).
2. S. Ozawa, and J. Tsuchiya, Research on Maglev Trains. JR Research Note No. 1281, Nov.(1984)(in Japanese).
3. S. Aita, E. Mestreau, N. Montmayeur, F. Masbernat, Y. F. Wolfhugel and J. C. Dumas, CFD Aerodynamics of the French High-Speed Train, SAE Paper 920343, Feb. (1992).
4. M. J. Siclari, G. Carpenter and R. Ende, Navier-Stokes Computation for a Magnetically Levitated Vehicle (Maglev) in Ground Effect. AIAA Paper 93-2950, July, (1993).
5. T. Kaiden, S. Hosaka and T. Maeda, A Validation of Numerical Simulation with Field Testing of JR Maglev Vehicle. The International Conference on Speedup Technology for Railway and Maglev Vehicles, Nov. (1993), pp. 199-204.
6. T. Ogawa and K. Fujii, Numerical Simulation of Compressible Flows Induced by a Train Moving into a Tunnel. Computational Fluid Dynamics Journal, Vol. 3, No. 1, 1994.
7. T. Ogawa and K. Fujii, Numerical Simulation of Compressible Flow Induced by a Train Moving in a Tunnel, AIAA Paper 93-2951, July, (1991).
8. K. Fujii and Y. Tamura, Recent Applications of the FNS Zonal Methods to Complex Flow Problems. SAE 1992 Aerospace Transaction, Vol. 100, Journal of Aerospace, Part 2, (1993), pp. 2149-2158.
9. W. R. Van Dalsem and J. L. Steger, Using the Boundary-Layer Equations in Three-Dimensional Viscous Flow Simulation. Proc. AGARD Fluid Dynamics Panel Symposium on Application of CFD in Aeronautics, Apr. 7-10(1986).

10. K. Fujii, A Method to Increase the Accuracy of Vortical Flow Simulations. AIAA paper 88-2562, June, 1988.

11. K. Fujii, Unified Zonal Method Based on the Fortified Solution Algorithm. ISAS Report No. 648, December, 1992.

12. K. Fujii and S. Obayashi, High-Resolution Upwind-Scheme for Vortical Flow Simulations. J. Aircraft, Vol. 26, No. 12, Dec., (1989), pp. 1123-1130.

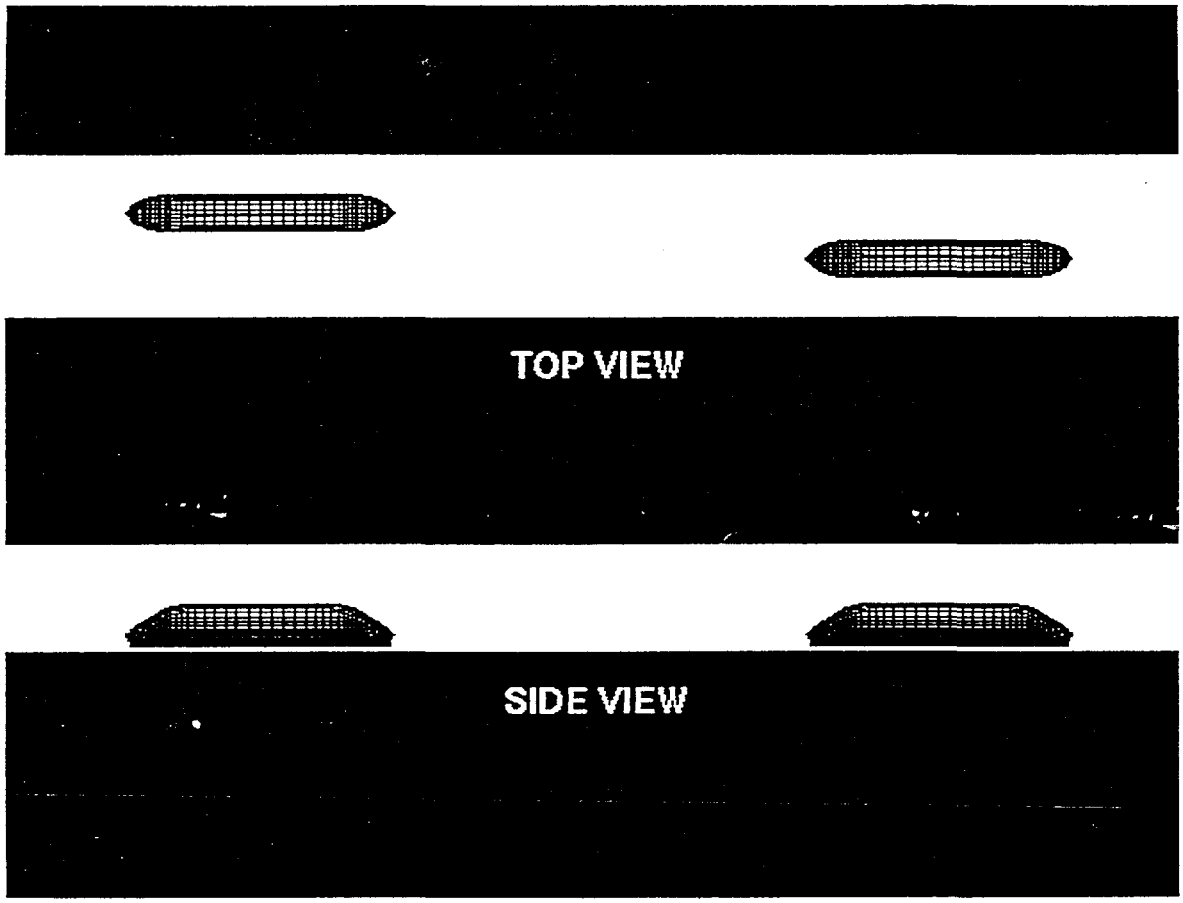

Fig. 1

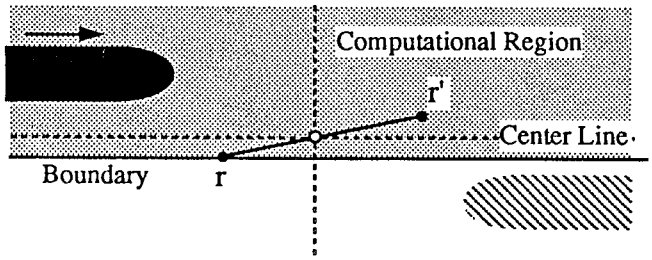

Fig. 2

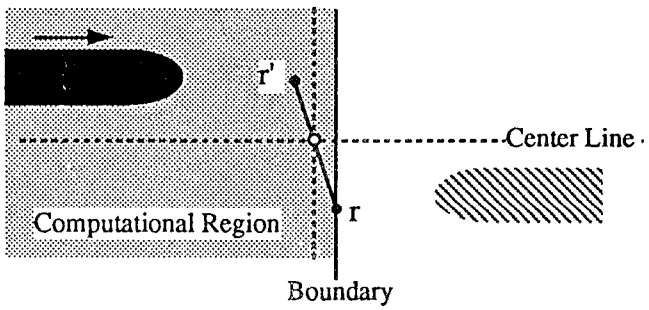

Fig. 3

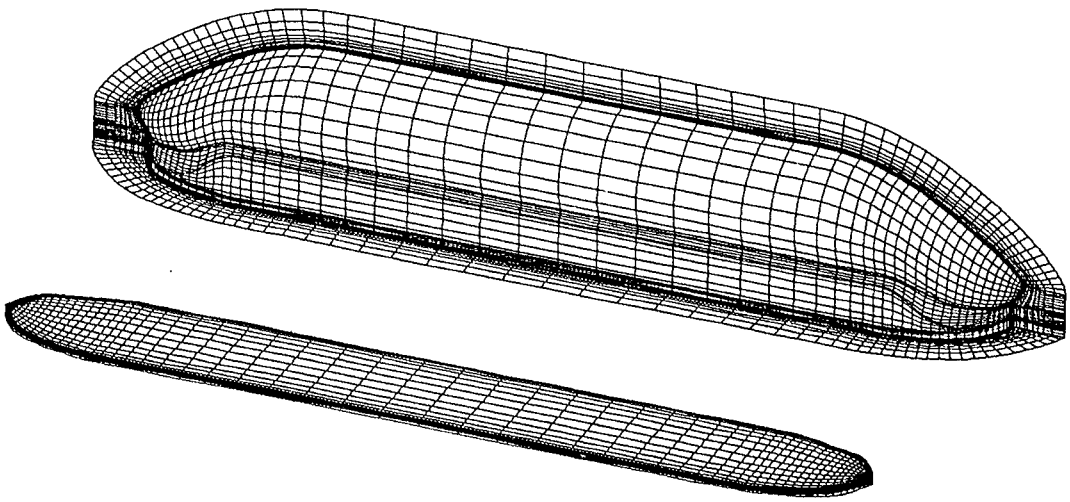

Fig. 4

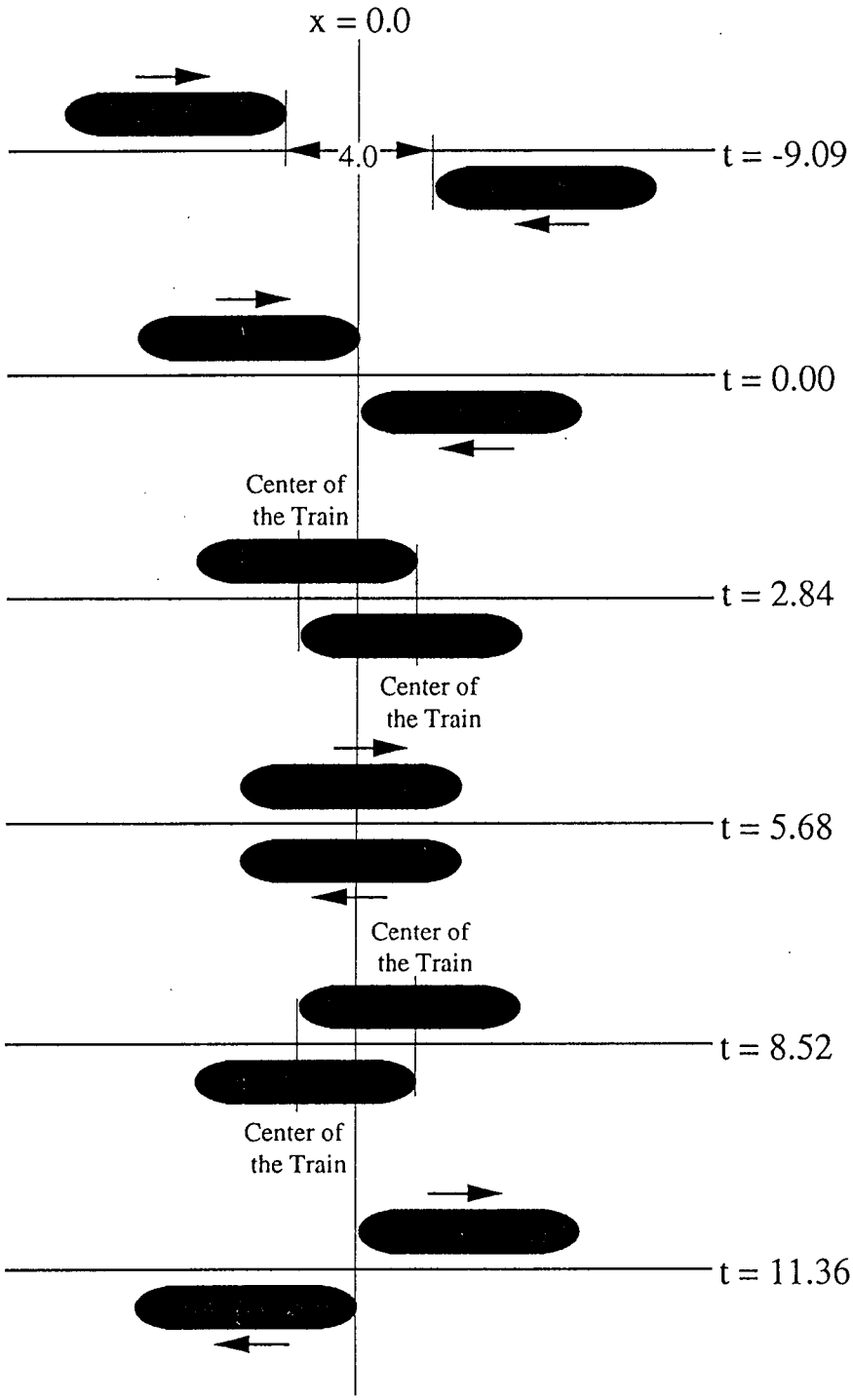
x = 0.0
4.0
t = -9.09
t = 0.00
Center of
the Train
t = 2.84
Center of
the Train
t = 5.68
Center of
the Train
t = 8.52
Center of
the Train
t = 11.36

Fig. 5

a)

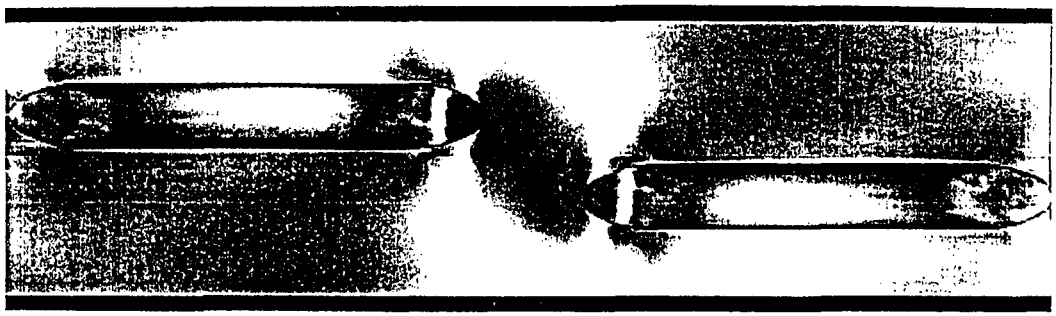

t=-1.09

b)

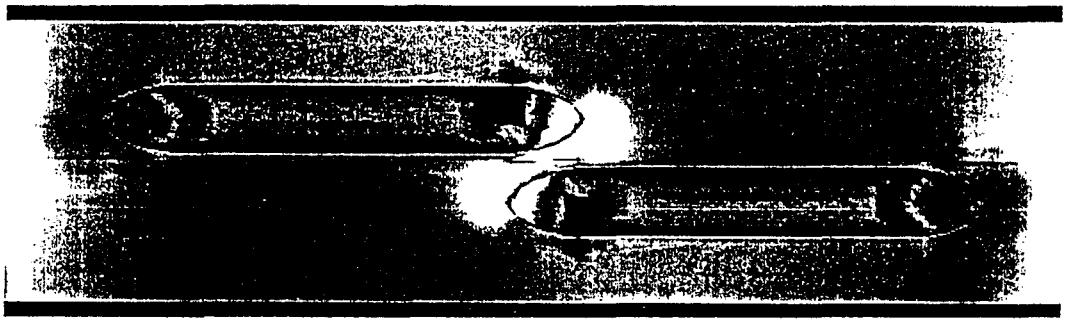

t=0.91

c)

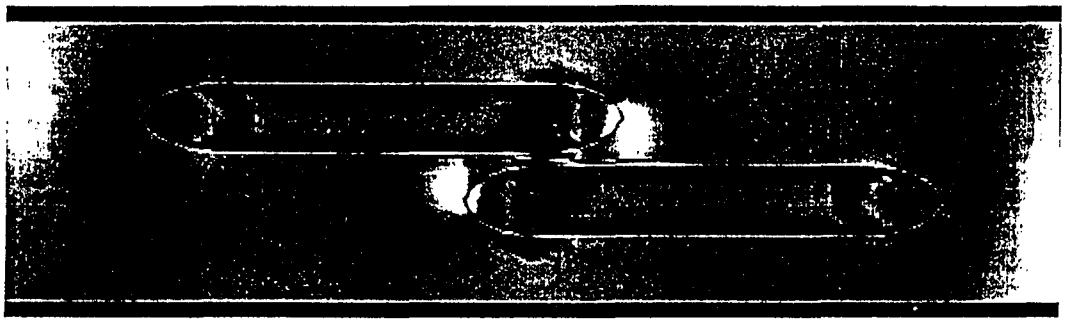

t=1.91

d)

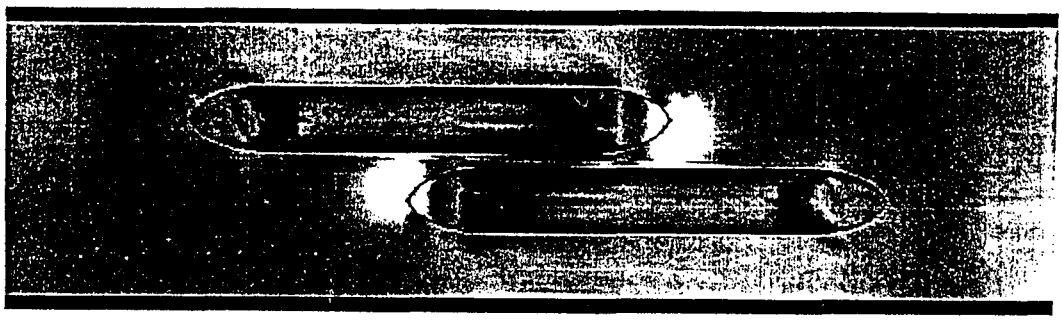

t=3.11

Fig. 6 Continued

e)

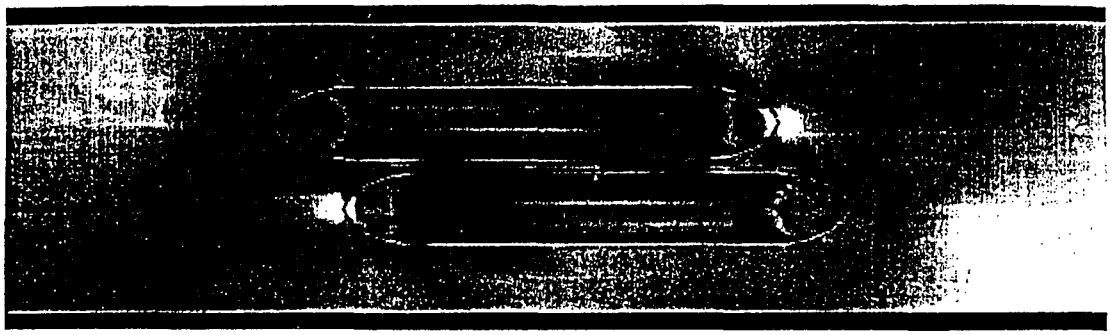

t=4.91

f)

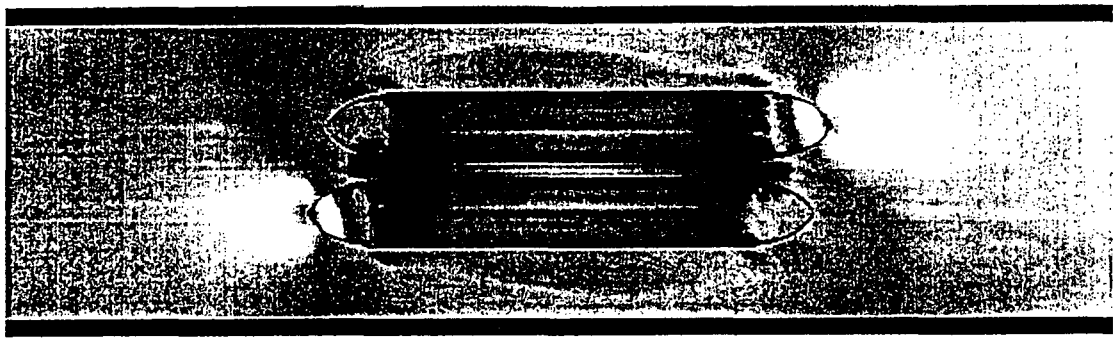

t=5.91

g)

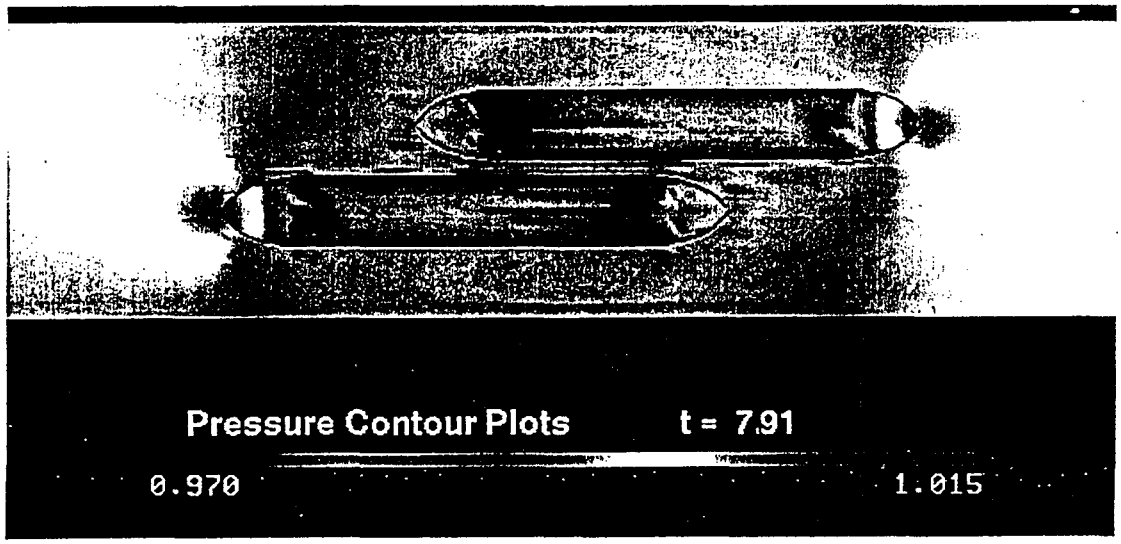

t=7.91

Fig. 6 Continued

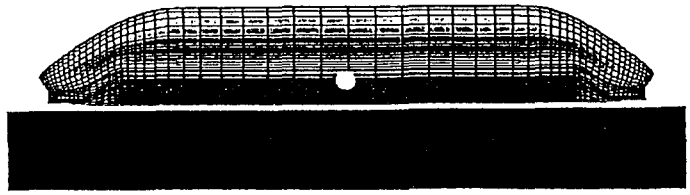

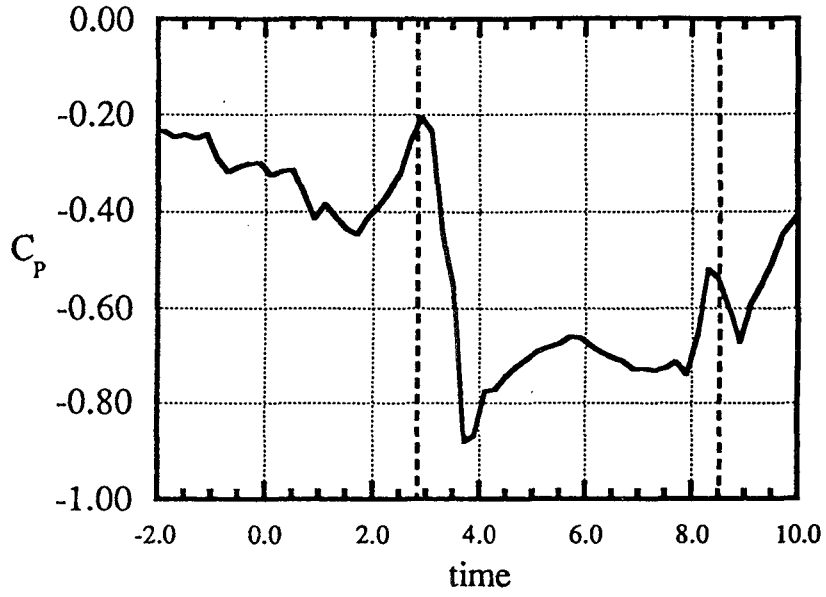

Fig. 7

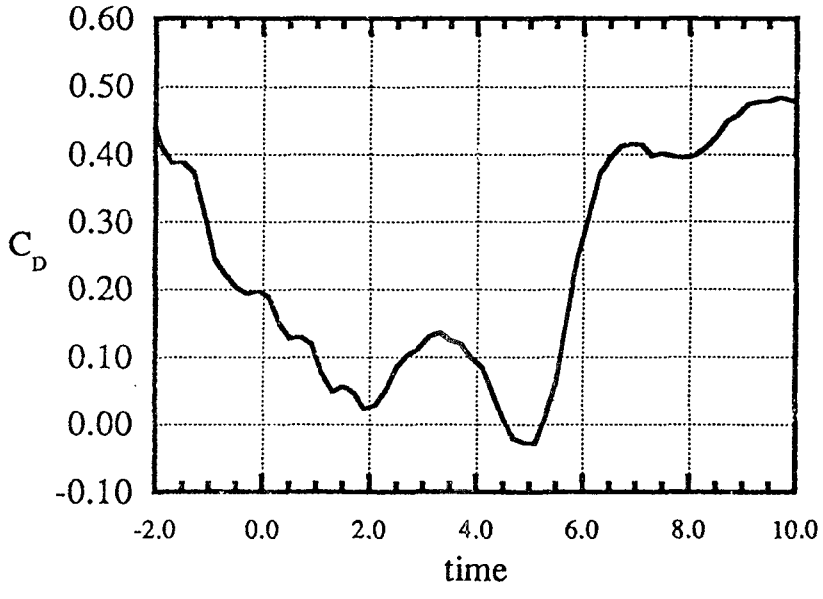

a)

Fig. 8 Continued

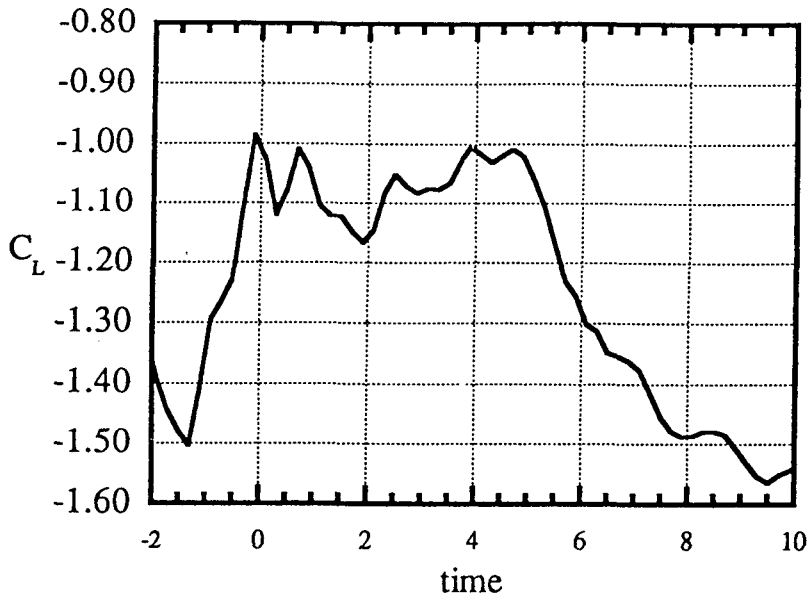

b)

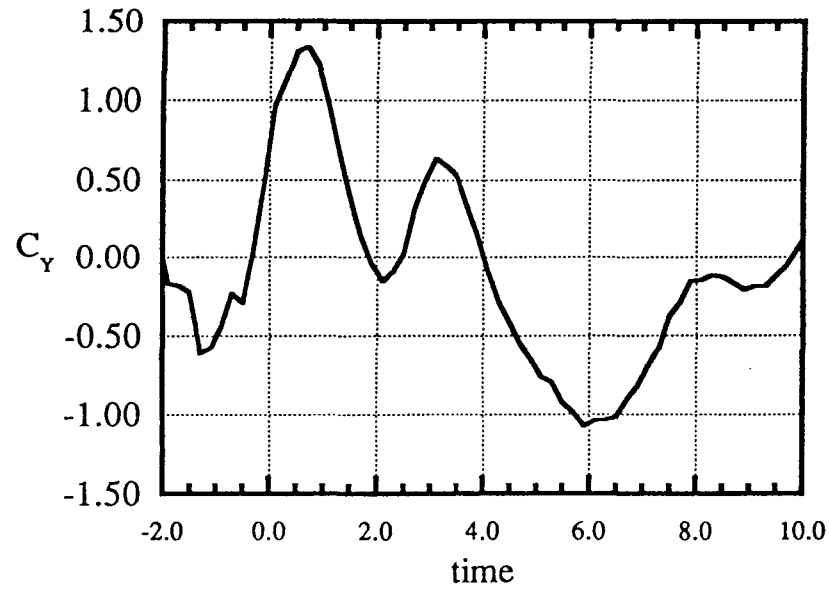

c)

Fig. 8 Continued

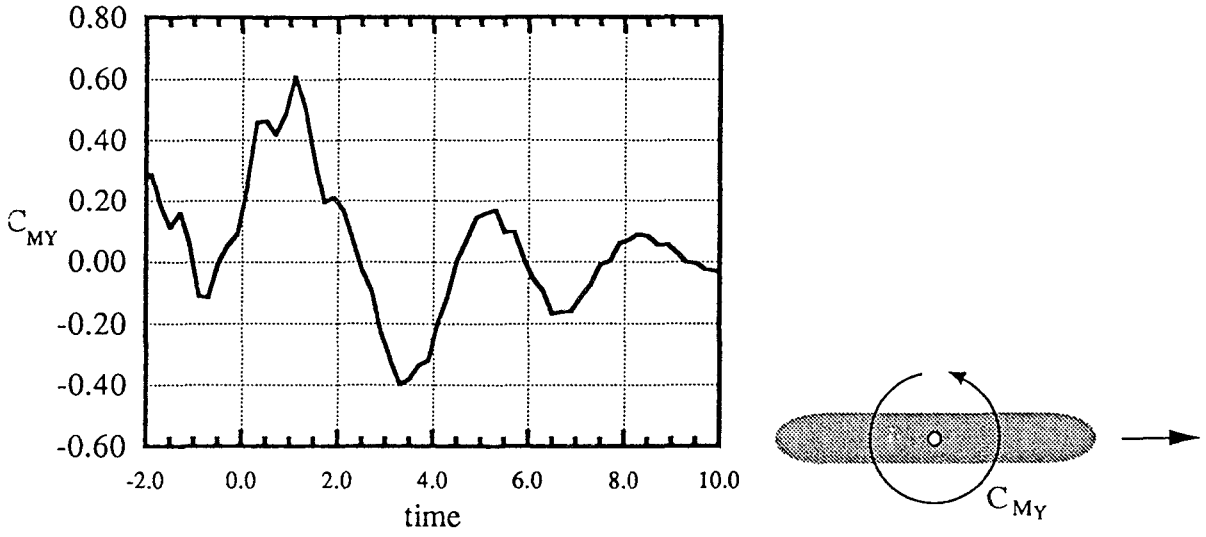

d)

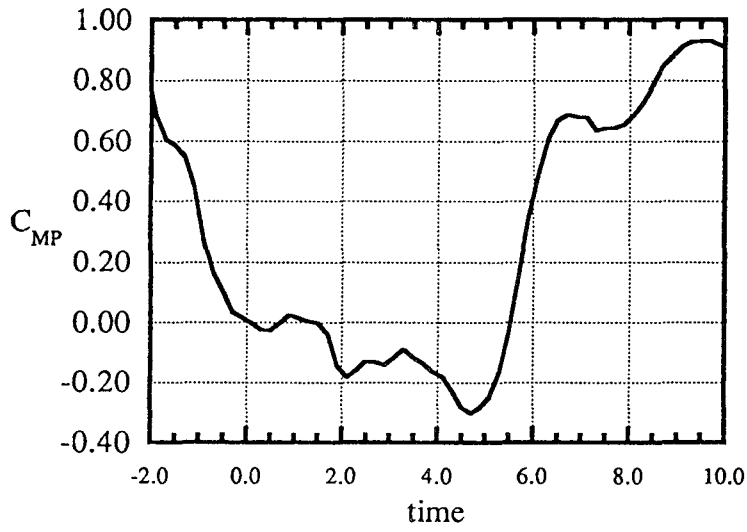

e)

Fig. 8 Continued

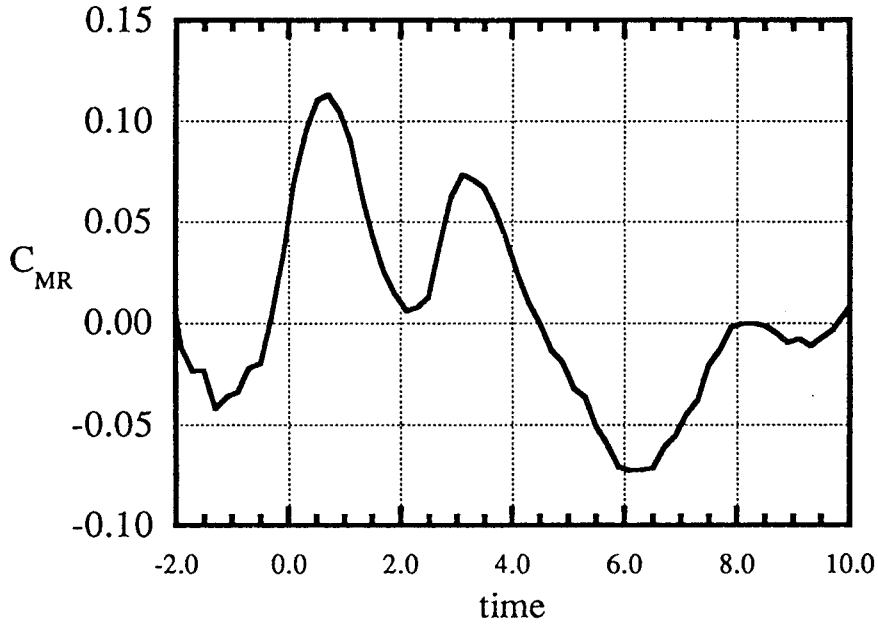

f)

Fig. 8 Continued

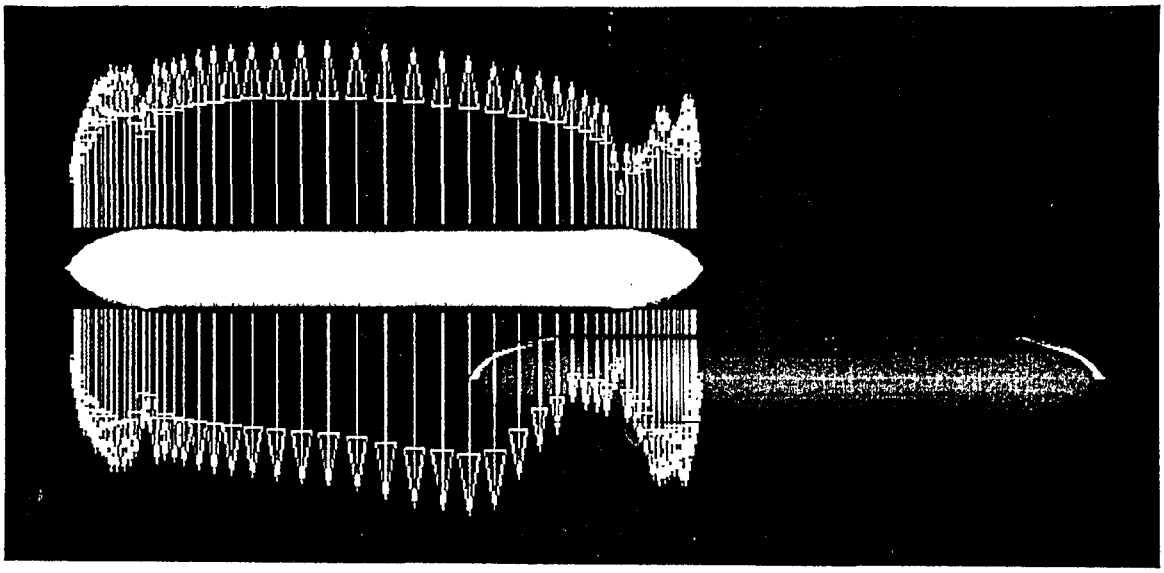

t=2.1

a)

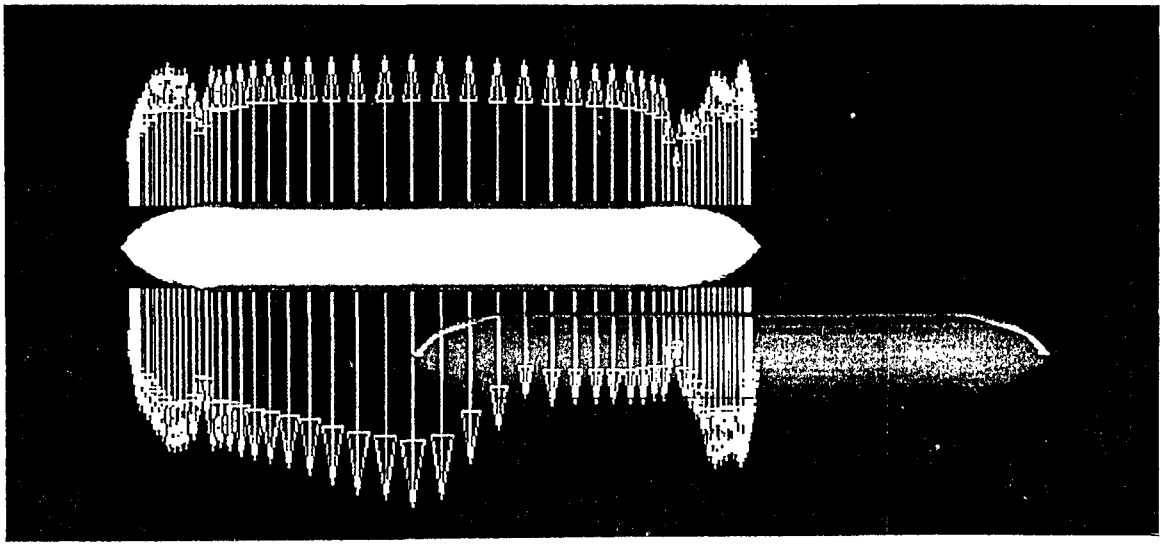

t=3.1

b)

Fig. 9